density increases. This is reasonable, since the cooling timescale of the X-ray gas is long compared with the dynamical timescale of the system (see above). Thus, from the X-ray derivation, the average density in the region producing the bulk of the optical emission lines should be $n_o = n_X T/T_o \approx 30–100\, n_X$ or about 1,700–5,000 cm^{-3}. These values are consistent with the optical model. The difference between the shock velocities in the optical model and that derived for the X-rays could be real or could indicate a somewhat lower X-ray temperature, $T \approx 0.6 \times 10^6$ K. A consistent theory of the emission from HH2H from optical through X-rays appears within reach.

However, it is also possible that while the X-ray emission arises from shock-heated post-shock fluid, the optical emission is dominated by a reverse shock propagating back into the fast material entering the HH2H region from the source (upstream) direction. On a much larger and faster scale, reverse shocks[23] are successful in explaining emission from supernova remnants. If the fast-moving upstream fluid is much denser than the downstream fluid before entering the reverse shock, the reverse shock speed will be much lower than the forward shock speed, and the post-shock material will predominantly radiate in lower excitation ultraviolet, optical and infrared lines. Deeper X-ray observations and nearly simultaneous optical images are needed to determine if the hot and relatively tenuous X-ray plasma does indeed lie at the leading (downstream) edge of the HH2H shock. □

Received 11 May; accepted 5 September 2001.

1. Herbig, G. H. The spectra of two nebulous objects near NGC 1999. *Astrophys. J.* **113,** 697–698 (1951).
2. Haro, G. Herbig's nebulous objects near NGC 1999. *Astrophys. J.* **115,** 572–573 (1952).
3. Ambarzumian, V. A. *Commun. Burakan Obs.* **13,** 3–35 (1954).
4. Canto, J. & Rodriguez, L. A stellar wind focusing mechanism as an explanation for Herbig–Haro objects. *Astrophys. J.* **239,** 982–987 (1980).
5. Schwartz, R. D. A shocked cloudlet model for Herbig–Haro objects. *Astrophys. J.* **233,** 884–900 (1978).
6. Norman, C. & Silk, J. Interstellar bullets: H_2O masers and Herbig–Haro objects. *Astrophys. J.* **228,** 197–205 (1979).
7. Reipurth, B. & Bertout, C. (eds) *Herbig–Haro Flows and the Birth of Stars* (IAU Symp. 182, Kluwer, Chamonix, France, 1997).
8. Pravdo, S. H. & Marshall, F. E. An X-ray active region in Orion: X-rays from a Herbig–Haro object? *Astrophys. J.* **248,** 591–595 (1981).
9. Ortalini, S. & Ordorico, S. A discussion on the nature of the Herbig Haro object no. 1 from its far UV spectrum. *Astron. Astrophys.* **83,** L8–L9 (1980).
10. Pravdo, S. H. *et al.* Detection of radio continuum emission from the Herbig–Haro objects 1 and 2 and from their central exciting source. *Astrophys. J.* **293,** L35–L38 (1985).
11. Bautz, M. W. *et al.* X-ray CCD calibration for the AXAF CCD imaging spectrometer. *Proc. SPIE* **3444,** 210–224 (1998).
12. Chandra Interactive Analysis of Observations (CIAO), http://asc.harvard.edu/ciao/, CIAO 2 Science Threads, Detecting Sources in Imaging Observations.
13. *The Hipparcos and Tycho Catalogs* Vols 1–17 (ESA SP-1200, European Space Agency, 1997).
14. Høg, E. *et al.* The Tycho-2 catalogue of the 2.5 million brightest stars. *Astron. Astrophys.* **35,** L27–L30 (2000).
15. Monet, D. G. The 526,280,881 objects in the USNO-A2.0 catalog *Am. Astron. Soc.* **193,** 12003 (1998).
16. Rodriguez, L. F. *et al.* New VLA observations of the HH 1-2 region: evidence for density enhancements moving along the axis of the VLA 1 radio jet. *Astrophys. J.* **119,** 882–889 (2000).
17. Mewe, R., Gronenschild, E. B. H. M. & van den Oord, G. H. J. Calculated X-radiation from optically thin plasmas. V. *Astron. Astrophys.* **62,** 197–254 (1985).
18. Böhm, K. H. & Brugel, E. W. The iron abundance in Herbig–Haro objects and some new spectrophotometric data on H-H 2H. *Astron. Astrophys.* **74,** 297–301 (1979).
19. Böhm-Vitense, E., Böhm, K. H., Cardelli, J. A. & Nemec, J. M. The ultraviolet and continuous emission of the Herbig–Haro objects HH 2 and HH 1. *Astrophys. J.* **262,** 224–233 (1982).
20. Eislöffel, J., Mundt, R. & Böhm, K.-H. Structure and proper motions in Herbig–Haro objects 1 and 2. *Astron. J.* **108,** 1042–1055 (1994).
21. Cox, D. P. & Daltabuit, E. Radiative cooling of a low-density plasma. *Astrophys. J.* **167,** 113–117 (1971).
22. Hartigan, P., Raymond, J. & Hartmann, L. Radiative bow shock models of Herbig Haro objects. *Astrophys. J.* **316,** 323–348 (1987).
23. McKee, C. F. X-ray emission from an inward-propagating shock in young supernova remnants. *Astrophys. J.* **188,** 335–339 (1974).

Acknowledgements

We thank L. Townsley and P. Broos for their assistance. We also thank B. Reipurth and R. Blandford for helpful discussions. This research was performed in part by the Jet Propulsion Laboratory, California Institute of Technology, under contract with the National Aeronautics and Space Administration.

Correspondence and requests for materials should be addressed to S.P. (e-mail: spravdo@jpl.nasa.gov).

Suppression of crystal nucleation in polydisperse colloids due to increase of the surface free energy

Stefan Auer & Daan Frenkel

FOM Institute for Atomic and Molecular Physics, Kruislaan 407, 1098 SJ Amsterdam, The Netherlands

The formation of small crystallites is governed by two competing factors: the free energy gained upon transferring constituent atoms, molecules or colloidal particles from the metastable liquid to the more stable solid, and the free energy needed to create the surface area of the crystallite[1]. Because the ratio of surface area to bulk is large for small particles, small crystallites dissolve spontaneously under conditions where larger crystallites are stable and macroscopic crystal growth occurs only if spontaneously formed crystallites exceed a critical minimum size. On theoretical grounds[1], the probability of forming such critical crystal nuclei is expected to increase rapidly with supersaturation. However, experiments show[1,2] that the rate of crystal nucleation in many systems goes through a maximum as the supersaturation is increased. It is commonly assumed that the nucleation rate peaks because, even though the probability of forming critical nuclei increases with increasing concentration, the rate of growth of such nuclei decreases. Here we report simulations of crystal nucleation in suspensions of colloidal spheres with varying size distributions that show that the probability that critical nuclei will form itself goes through a maximum as the supersaturation is increased. We find that this effect, which is strongest for systems with the broadest particle size distribution, results from an increase with supersaturation of the solid–liquid interfacial free energy. The magnitude of this effect suggests that vitrification at high supersaturations should yield colloidal glasses that are truly amorphous, rather than nano-crystalline.

Colloidal suspensions of identical, hard, spherical particles can be either fluid or crystalline. At low densities, the fluid state is stable, but when the colloids occupy more than 49.4% of the volume, a crystalline phase should form[2]. In practice, several factors influence the crystallization of hard-sphere colloids. First of all, synthetic colloids have a distribution of particle radii with a width that is rarely less than 2–3% of the average radius. This non-uniformity of size ("polydispersity") is known to affect the location of the freezing curve. Simulations[3] show that higher compressions are needed to freeze a polydisperse suspension. Irrespective of the composition of the coexisting fluid, the polydispersity of the crystal never exceeds 5.7%. Experiments on crystal formation in hard-sphere colloids indicate that crystallization is suppressed in suspensions with a polydispersity exceeding 12% (ref. 2). This must be due to kinetic factors, as crystallization of strongly polydisperse suspensions is not excluded on thermodynamic grounds.

Classical nucleation theory (CNT)[1] offers a simple thermodynamic explanation for why small crystal nuclei are less stable (that is, they have a higher free energy) than the supersaturated parent phase. CNT uses macroscopic arguments to estimate the free energy required to form a crystallite. The decrease in free energy due to the transfer of N particles from the metastable liquid to the solid state is approximated as $N\Delta\mu$, where $\Delta\mu = \mu_{solid} - \mu_{liquid}$ is the difference in chemical potential between the solid and the liquid state. The CNT estimate for the free-energy cost involved in the creation of the surface area A of the nucleus is γA, where γ is the surface free energy of the solid–liquid interface.

Owing to the competition between bulk and surface terms, the Gibbs free energy $\Delta G(N)$ required to form an N-particle nucleus

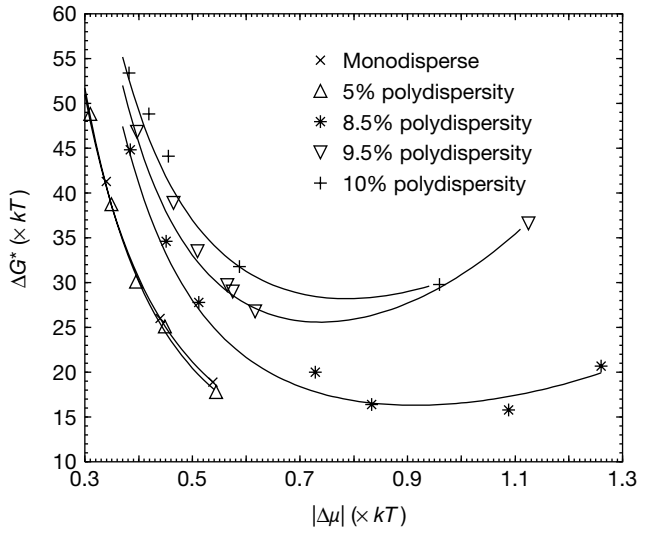

Figure 1 Computed free-energy barrier for crystal nucleation of polydisperse suspensions of hard, colloidal spheres. The free energy ΔG^* is expressed in terms of kT, where k is Boltzmann's constant and T is the absolute temperature. $|\Delta\mu|$ (also in terms of kT) is the absolute difference between the chemical potential of the liquid and the solid. It is a measure for the degree of supersaturation. The curves are fits that have been drawn as a guide to the eye. To facilitate comparison with experiment, we show, in Table 1, the relationship between $|\Delta\mu|$ and the volume fraction φ of the liquid for the different systems that we studied.

goes through a maximum at a value of N called the critical nucleus size. For a spherical nucleus, the maximum value of $\Delta G(N)$ is:

$$\Delta G^* = (16\pi/3)\gamma^3/(\rho|\Delta\mu|)^2 \quad (1)$$

where ρ is the number density of the crystal phase. The rate I at which nuclei are formed depends exponentially on ΔG^*:

$$I = \kappa \exp(-\Delta G^*/kT) \quad (2)$$

where T is the absolute temperature, k is Boltzmann's constant and κ is a kinetic prefactor that is proportional to the short-time self-diffusion constant of the colloids. The form of equation (2) does not rely on the validity of CNT.

In the CNT picture, increasing the supersaturation (that is, increasing $|\Delta\mu|$) lowers the nucleation barrier. If γ were independent of $|\Delta\mu|$, then ΔG^* would always decrease with increasing supersaturation. In experiments[4–6] the rate of colloidal crystal nucleation starts to decrease again for large supersaturations. This effect is attributed to the decrease in the kinetic prefactor κ: in order to crystallize, colloidal fluids must be compressed beyond the freezing curve. But eventually, the suspension will vitrify under compression. This vitrification slows down the particle motion and presumably reduces κ in equation (2). A problem with this interpretation is that recent experiments on colloidal crystallization in micro-gravity have found evidence for crystallization at densities that are well beyond the glass transition point[7].

We performed Monte Carlo simulations to study the crystal-nucleation barrier and the structure of the critical nucleus, as a function of both polydispersity and supersaturation. As in the case of monodisperse suspensions[8], we find that all critical nuclei have a randomly stacked close-packed structure. During crystallization, size-fractionation occurs[3]: the particles that make up the critical nucleus are on average larger than those in the metastable liquid. At fixed $|\Delta\mu|$ we find that ΔG^*, the height of the nucleation barrier, does not depend on the polydispersity for polydispersities $\leq 5\%$ (see Fig. 1). As the polydispersity is increased beyond 5%, ΔG^* increases rapidly. This implies that the probability of a critical nucleus forming is suppressed in polydisperse suspensions. It follows from equation (1) (or actually, from its polydisperse equivalent) that, at constant $|\Delta\mu|$, the variation of ΔG^* with polydispersity is due to an increase of the interfacial free energy γ. The increase of γ with polydispersity runs counter to Turnbull's suggestion that the interfacial free energy should be proportional to ΔH, the latent heat of fusion[1]. For the systems that we studied, ΔH crosses zero at a polydispersity of about 9%, where the liquid becomes denser than the coexisting solid[3]. Yet, γ clearly remains non-zero.

Surprisingly, the variation of ΔG^* with $|\Delta\mu|$ is non-monotonic. As $|\Delta\mu|$ is increased, the nucleation barrier goes through a minimum (Fig. 1). This non-monotonic behaviour of ΔG^* is due to the increase of γ with $|\Delta\mu|$ (Fig. 2). To illustrate this, let us approximate the $|\Delta\mu|$-dependence of γ by $\gamma \approx \gamma_0(1 + \alpha|\Delta\mu|)$. If we disregard the slight $|\Delta\mu|$-dependence of the solid density, it then follows from equation (1) that ΔG^* must go through a minimum when $|\Delta\mu| = 2/\alpha$. The nucleation theorem[9] suggests that the minimum in ΔG^* is due to the inversion of the number densities of the polydisperse fluid and the crystal nucleus. In CNT it is usually assumed that γ is constant. A linear variation of γ with $|\Delta\mu|$ has been observed in inorganic glasses[1], but there the constant α is negative and hence there is no minimum in ΔG^*. In other systems[10,11], non-monotonic behaviour of ΔG^* is induced by a hidden phase transition in the metastable phase.

The minimum value of ΔG^* increases rapidly with polydispersity. Using kinetic Monte Carlo simulations, we can estimate the value of

Table 1 Supersaturation and volume fraction of polydisperse colloids

0%		5%		8.5%		9.5%		10%	
$\Delta\mu$	φ	$\Delta\mu$	φ	$\Delta\mu$	φ	$\Delta\mu$	φ	$\Delta\mu$	φ
0.339	0.5207	0.310	0.5344	0.385	0.5614	0.397	0.5697	0.382	0.5717
0.439	0.5277	0.349	0.5377	0.451	0.5673	0.465	0.5746	0.419	0.5738
0.538	0.5342	0.395	0.5414	0.512	0.5726	0.509	0.5782	0.455	0.5775
		0.448	0.5456	0.728	0.5864	0.565	0.5808	0.587	0.5878
		0.544	0.5528	0.833	0.5948	0.575	0.5828	0.959	0.6239
				1.088	0.6145	0.616	0.5859		
				1.260	0.6212	1.125	0.6239		

$\Delta\mu$ is the supersaturation and φ is the volume fraction of the colloidal fluid. Pairs of values are given for polydispersities in the range from 0% (left) to 10% (right). The polydispersities quoted in Table 1 and in Figs 1 and 2 are those of the metastable liquid.

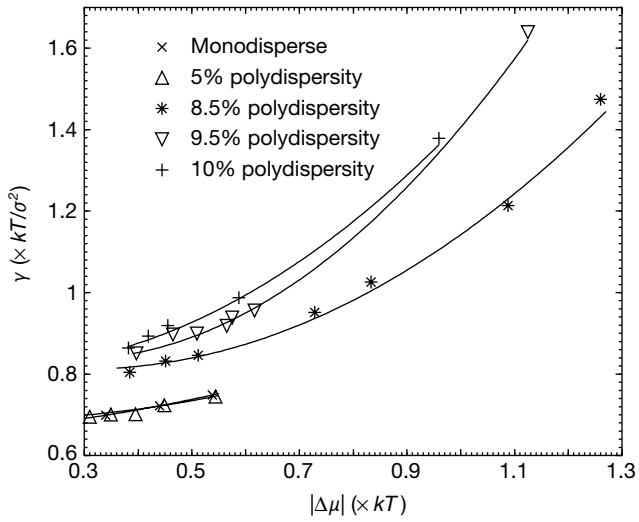

Figure 2 The interfacial free energy of crystal nuclei in polydisperse suspensions of hard, colloidal spheres. The interfacial free energy γ is expressed in terms of kT/σ^2, where σ is the average hard-sphere diameter. The curves are fits that have been drawn as a guide to the eye.

the kinetic prefactor[8]. We find that, over the range of supersaturations studied, the kinetic prefactors vary by at most an order of magnitude (S.A. and D.F., manuscript in preparation). This means that the variation in the rate of nucleation is dominated by the behaviour of ΔG^*. We estimate that, for colloidal particles with a radius $\geq$500 nm, homogeneous nucleation will be effectively suppressed (less than one nucleus per cubic centimetre per day) when the polydispersity exceeds 10%. This finding has important implications for the morphology of polycrystalline colloidal materials. Using a simplified version of the analysis proposed in ref. 10 to estimate the size of crystallites in a polycrystalline sample, it is easy to derive that R_c, the average crystallite size at the end of a nucleation experiment, should scale as $\exp(\Delta G^*/4kT)$. Our observation of a minimum in ΔG^* thus implies the existence of a minimum in the typical crystallite size. This should be experimentally observable.

We could only compute ΔG^* if spontaneous nucleation did not occur in the course of a simulation. In practice, this implied that we could not study barriers lower than $15kT$. As a result, we could not test whether ΔG^* in systems with a low polydispersity (less than 8.5%) also has a minimum. If we assume that at lower polydispersities we can extrapolate the increase of γ with $|\Delta\mu|$ to large supersaturations, then we predict that a minimum in ΔG^* should occur even in nearly monodisperse systems. Again, this should be experimentally observable, because we should expect to see the formation of larger crystallites if the solution can be compressed rapidly through the region where ΔG^* is small.

There are two ways to interpret the experimental finding that crystallization is not observed in suspensions with a polydispersity greater than 12%: either crystals do not form, or they are too small to be observed. Our simulations support the first interpretation. In a suspension of colloids with a 500-nm radius, we would expect[10] to see less than one crystallite per cubic centimetre, once $\Delta G^* > 32kT$. In other words, under those conditions the colloidal glass is truly amorphous.

Our predictions concerning the structure and free energy of colloidal crystal nuclei can be tested experimentally. Recently, the technique of confocal scanning laser microscopy has been used[12] to study the structure and size of critical crystal nuclei in dense colloidal suspensions and would thus be perfectly suited to test our predictions. Our prediction concerning the minimum in ΔG^* is even easier to verify. By visual inspection, one could verify whether the crystallites that nucleate in strongly supersaturated solutions are larger than those that form at lower supersaturations. Over a decade ago, Pusey and van Megen produced images of the morphology of polycrystalline hard-sphere colloids[13] and similar morphologies have recently been observed in a study of colloidal crystallization in micro-gravity (Z. D. Cheng, W. B. Russel and P. M. Chaikin, unpublished data). The observed increase of the crystallite size at large supersaturations was attributed to heterogeneous nucleation[13], so a direct test of our prediction is still lacking. □

Methods

The simulation techniques that are required to compute the free energy of small crystal nuclei have been described in earlier publications[8,14]. In the present work, we used constant-pressure, semi-grand-canonical Monte Carlo (SGMC) simulations of the type described in ref. 3. To eliminate possible finite-size effects, we used systems of 3,375 particles. Very long runs (up to 1.6×10^7 trial moves per particle), in combination with parallel tempering[8], were needed to ensure equilibration of the dense, polydisperse fluid.

Received 16 July; accepted 3 September 2001.

1. Kelton, K. F. *Solid State Physics* Vol. 45 (eds Ehrenreich, H. & Turnbull, D.) 75–178 (Academic, New York, 1991).
2. Pusey, P. in *Liquids, Freezing and Glass Transition* (eds Hansen, J. P., Levesque, D. & Zinn-Justin, J.) 763–931 (North-Holland, Amsterdam, 1991).
3. Kofke, D. A. & Bolhuis, P. G. Freezing of polydisperse hard spheres. *Phys. Rev. E* **59,** 618–622 (1999).
4. Palberg, T. Crystallization kinetics of repulsive colloidal spheres. *J. Phys. Condens. Matter* **11,** 323–360 (1999).
5. Van Duijneveldt, J. S. & Lekkerkerker, H. N. W. in *Science and Technology of Crystal Growth* (eds van der Eerden, J. P. & Bruinsma, O. S. L.) 279–290 (Kluwer Academic, Dordrecht, 1995).
6. Harland, J. L. & Van Megen, W. Crystallization kinetics of suspensions of hard colloidal spheres. *Phys. Rev. E* **55,** 3054–3067 (1997).
7. Zhu, J. *et al.* Crystallization of hard-sphere colloids under microgravity. *Nature* **387,** 883–885 (1997).
8. Auer, S. & Frenkel, D. Prediction of absolute crystal-nucleation rate in hard-sphere colloids. *Nature* **409,** 1020–1023 (2001).
9. Oxtoby, D. W. & Kashchiev, D. A general relation between the nucleation work and the size of the nucleus in multicomponent nucleation. *J. Chem. Phys.* **100,** 7665–7671 (1994).
10. Shi, F. G., Tong, H. Y. & Ayers, J. D. Free energy barrier to nucleation of amorphous-to-crystalline transformation selects the scale of microstructure of crystallized materials. *Appl. Phys. Lett.* **67(3),** 350–352 (1995).
11. Ten Wolde, P. R. & Frenkel, D. Enhancement of protein crystal nucleation by critical density fluctuations. *Science* **277,** 1975–1978 (1997).
12. Gasser, U., Weeks, E. R., Schofield, A., Pusey, P. N. & Weitz, D. A. Real-space imaging of nucleation and growth in colloidal crystallization. *Science* **292,** 258–262 (2001).
13. Pusey, P. N. & Van Megen, W. Phase behaviour of concentrated suspensions of nearly hard colloidal spheres. *Nature* **320,** 340–342 (1986).
14. Ten Wolde, P. R., Ruiz-Montero, M. J. & Frenkel, D. Numerical evidence for bcc ordering at the surface of a critical fcc nucleus. *Phys. Rev. Lett.* **75,** 2714–2717 (1995).

Acknowledgements

We thank A. van Blaaderen, P. M. Chaikin, H. N. W. Lekkerkerker, D. Oxtoby, W. B. Russel and F. Shi for comments and suggestions. This work was supported by the division of Chemical Sciences of the Netherlands Organization for Scientific Research (NWO). The work of the FOM Institute is part of the research programme of FOM and is made possible by financial support from the NWO. Access to the TERAS supercomputer was made possible through a grant by the NCF.

Correspondence and requests for materials should be addressed to D.F. (e-mail: Frenkel@amolf.nl).

Self-assembled monolayer organic field-effect transistors

Jan Hendrik Schön, Hong Meng & Zhenan Bao

Bell Laboratories, Lucent Technologies, Mountain Avenue, Murray Hill, New Jersey 07974, USA

The use of individual molecules as functional electronic devices was proposed in 1974 (ref. 1). Since then, advances in the field of nanotechnology have led to the fabrication of various molecule devices and devices based on monolayer arrays of molecules[2–11]. Single molecule devices are expected to have interesting electronic properties, but devices based on an array of molecules are easier to fabricate and could potentially be more reliable. However, most of the previous work on array-based devices focused on two-terminal structures: demonstrating, for example, negative differential resistance[8], rectifiers[9], and re-configurable switching[10,11]. It has also been proposed that diode switches containing only a few two-terminal molecules could be used to implement simple molecular electronic computer logic circuits[12]. However, three-terminal devices, that is, transistors, could offer several advantages for logic operations compared to two-terminal switches, the most important of which is 'gain'—the ability to modulate the conductance. Here, we demonstrate gain for electronic transport perpendicular to a single molecular layer (~10–20 Å) by using a third gate electrode. Our experiments with field-effect transistors based on self-assembled monolayers demonstrate conductance modulation of more than five orders of magnitude. In addition, inverter circuits have been prepared that show a gain as high as six. The fabrication of monolayer transistors and inverters might represent an important step towards molecular-scale electronics.

It has been shown that conjugated organic molecular materials behave very much like conventional semiconductors and various electronic devices have been demonstrated[13,14]. Although great progress has been made, the knowledge of the conduction mechanism on the molecular scale is not completely understood yet[5]. Nevertheless, the possibility of three-terminal devices using a benzene ring and other molecules has been proposed[15,16] and an